Postprint of: Rehman M., Hafeez M. B., Krawczuk M., A Comprehensive Review: Applications of the Kozeny–Carman Model in Engineering with Permeability Dynamics, ARCHIVES OF COMPUTATIONAL METHODS IN ENGINEERING (2024)

A Comprehensive Review: Applications of the Kozeny-Carman Model in Engineering with Permeability Dynamics

Maryam Rehman[1], Muhammad Bilal Hafeez[2*], Marek Krawczuk[2]

[1]Department of Mathematics, Air University, P.A.F Complex E-9, Islamabad 44000, Pakistan.

[2]Gdansk University of Technology, Faculty of Mechanical Engineering and Ship Technology, Institute of Mechanics and Machine Design, Narutowicza 11/12, 80-233 Gdańsk, Poland.

Abstract:

In this review article, we investigate the dynamic nature of the Kozeny-Carman Model concerning permeability and its application in engineering contexts. Providing insights into the changing dynamics of permeability within mining, petroleum, and geotechnical engineering, among other engineering applications. While some are complex and require additional modifications to be applicable, others are simple and still function in specific situations. Therefore, having a thorough understanding of the most recent permeability evolution model would help engineers and researchers in finding the right solution for engineering issues for prospects. The permeability evolution model Kozeny-Carman (KC) put forth by previous and current researchers is compiled in this paper, with a focus on its features and drawbacks.

Keywords: Comprehensive Review Permeability Dynamics, Kozeny-Carman Model, Engineering Applications, Porous Media Studies, Fluid Flow Analysis.

Nomenclature

Δp	Pressure drop
L	Total height of the bed
K	Empirical constant
V_o	Superficial velocity
D_p	Diameter of the equivalent spherical particle
a_v	Specific surface of the bed
S_p	Particle's surface area
v_p	Volume

K_p	Permeability of porous media
S	Surface area per unit volume
B	Pore shape coefficient
c	Constant of permeability
z	Exponent variable
K_o	Initial permeability
V	Flow rate
L_M	Thickness of the membrane
D	Pore diameter
N	Mass velocity
D_H	Hydraulic diameter
P	Perimeter of the pore
A_p	Cross-sectional area of pore
P_M	Bulk-flow permeability
R_c	Barrier preventing the fluid from passing through the cake
R_M	Barrier preventing the fluid from passing through the membrane
L_c	Thickness of the cake
f_n	Sound frequency
z_b	Complex wave number
k_b	Characteristic impedance
c_o	Speed of sound in air
Z_s	normalized acoustic surface impedance
l_s	Thickness of polyester fiber
d	Particle size
d_f	Fiber diameter
v_{ave}	Average flow velocity
R	Radius of tube
i_h	Hydraulic gradient
R_H	Hydraulic radius of a circular tube
q_{cir}	Fluid's volume
a	Cross-sectional area of tube
C_s	Shape factor
A_f	Area of flow passage
A	Total cross-sectional area
n	Porosity of soil
P_c	Total circumference of the flow tubes
L_f	Length of the flow tube
V_w	Volume of water
V_s	Volume of solid
S_p	Specific surface area of particle
V_{ab}	Volume of absorbed water
V_v'	Effective pore volume
V_{noc}	Volume of pores
V_{unc}	Volume of unconnected pores
V_s'	Volume of soil and water

V_s	Volume of soil particles
e_{eff}	Effective volume

Greek letters

μ	Viscosity of the fluid
ϕ_s	Sphericity of the particles in the packed bed
ε	Packed bed's porosity
ϕ	Porosity of porous media
τ	Tortuosity of porous media
ϕ_o	Initial porosity
α	Porosity-sensitive exponent
ρ	Fluid density
$F(\sigma)$	Acoustic absorption coefficient
σ	Airflow resistivity
α_e	Experimental absorption coefficient
α_m	Predicted absorption coefficient
α_p	Absorption coefficient of polyester fiber
ρ_m	Material density
ρ_f	Density of polyester fiber
γ_p	Specific gravity
ρ_s	Density of soil
δ	Thickness of absorbed water

1. Introduction:

Over the past decade, a wide range of both empirical and theoretical approaches have been developed to understand better fluid flow and coupled flow-deformation challenges [1]. The Kozeny-Carman (KC) Model has become an important structure for understanding the development of permeability. This review compiles a large amount of literature on the KC Model, examines its advantages and disadvantages, and highlights its critical function in solving challenging engineering problems. However, this analysis shows researchers and engineers acquire a valuable tool for dealing with the complexities of permeability dynamics in real-world engineering problems. Activities related to geological and geotechnical engineering have had a major impact. Therefore, a variety of applications in reservoir, geotechnical, mining, and petroleum engineering depend on the dimensions to document the development in permeability studies under diverse conditions (thermal, mechanical, and chemical approaches) [2].

Researchers have explored the laws of permeability evolution, which involve porosity, stress, temperature, chemical processes, mass removal, and failure models in [3] and [4]. Models of permeability evolution can be broadly categorized into four families: (i) network model, (ii) analogous channel concept, (iii) stress and damage, and (iv) porosity. However, the models have their own limitations and can only be applied under specific conditions because of the intricate connections between compression and flow in geophysical and geotechnical sciences. To address fluid flow issues, research on models based on the evolution of permeability of fractured porous media is therefore crucial. Indeed, knowledge of the most recent permeability evolution model would be beneficial to engineers and researchers. Several articles have explored the impact of porous media on fluid flow analysis [5-10]. The primary goal of this article is to review the most recent advancements in the Kozeny-Carman model of porous media permeability evolution. This article is divided into five different sections such as Introduction, Models of Changes in Permeability Based on Porosity, Section Three on applications of the KC model, which was recently used, Section Four, Concluding Remarks, and the last one is the fifth section, which is on future prospectives. This article presents a pivotal contribution to the scientific community engaged in engineering disciplines, specifically focusing on permeability dynamics. The Kozeny-Carman model's significance lies in its applicability across diverse engineering fields, including civil, chemical, and petroleum engineering, among others. This review meticulously explores the model's versatility in predicting fluid flow through porous media, emphasizing its practical implications in numerous industrial processes, groundwater remediation, hydrocarbon recovery, and environmental engineering [11-15]. By delving into the model's adaptability and limitations in varying scenarios, this comprehensive review offers a critical evaluation, fostering advancements and encouraging innovative applications within the scientific community, thereby serving as a valuable resource for researchers, engineers, and practitioners seeking to optimize processes involving porous media and fluid flow dynamics. According to Scopus analysis, Fig 1. shows how many papers were published between 2010 and 2023 regarding porosity and permeability in relation to the Kozeny-Carman (KC) model; the results show a significant increase in the quantity of research conducted to investigate potential uses, modifications, and improvements of the KC model to comprehend fluid flow through porous media.

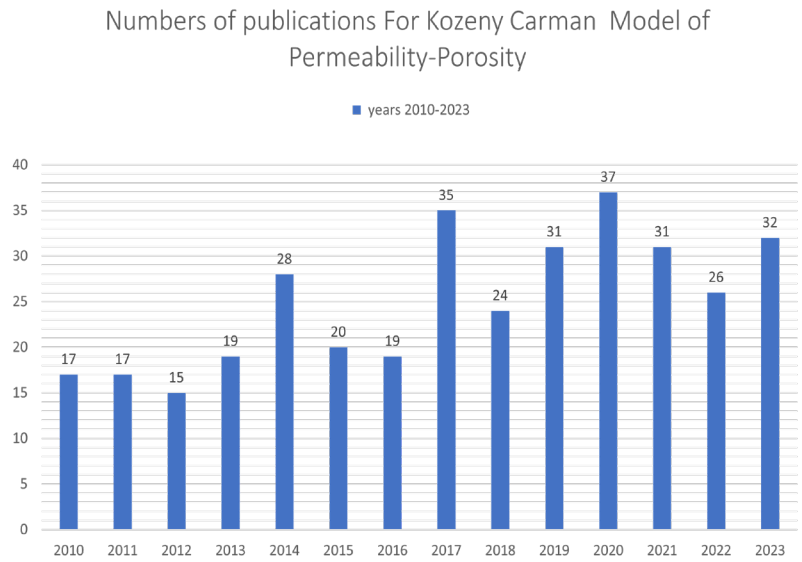

Figure 1. Number of publications for KC model of Permeability porosity from 2010-2023.

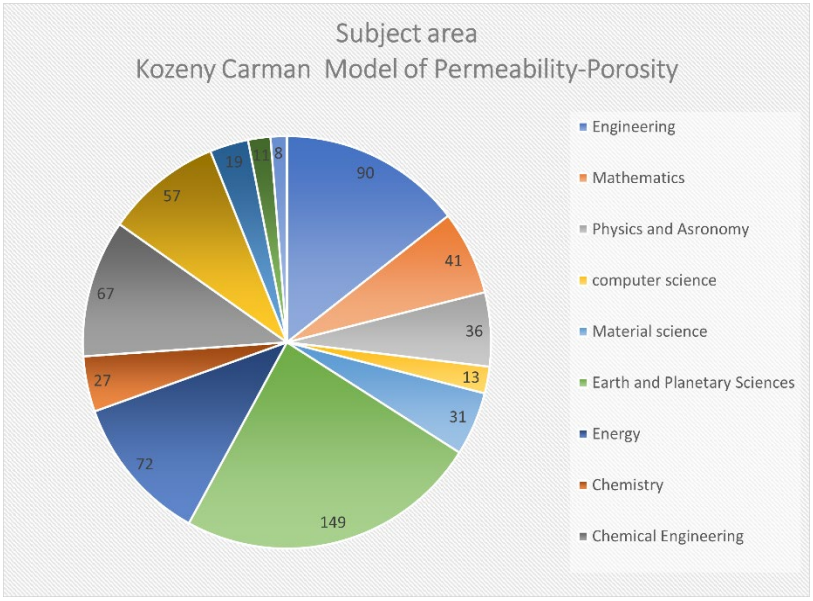

Figure 2. Number of publications for KC model of Permeability porosity regarding subject area.

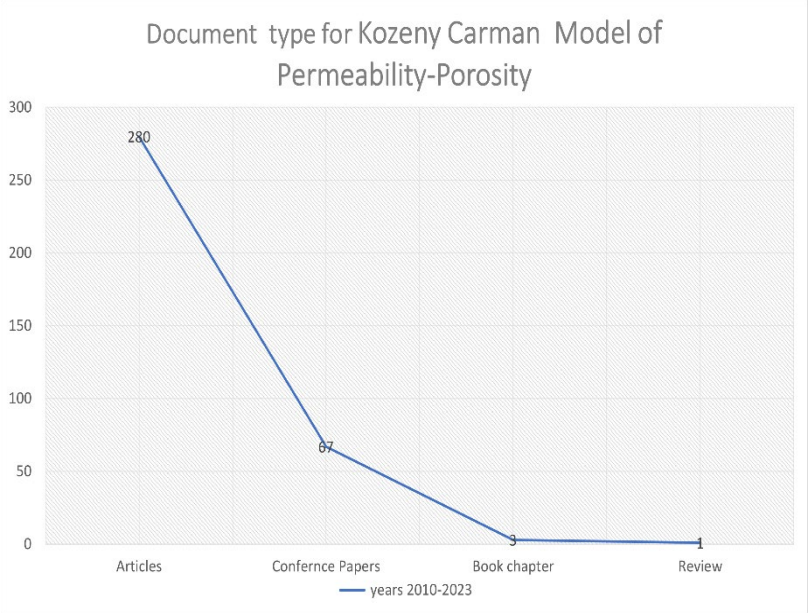

Figure 3. Document type for KC model of Permeability porosity from 2010-2023.

In Fig.2. and Fig.3. highlights the distribution of publications related to understanding porosity and permeability in various fields using the Kozeny-Carman (KC) model. This flow chart shows the interdisciplinary nature of the KC model and shows how widely applicable it is across a range of fields. It also indicates the level of interest and participation that academics from various disciplines, such as Engineering, Mathematics, Physics, Chemical science, and as well as in Material sciences, have shown in investigating the significance of the KC model for understanding fluid flow through porous media throughout the years from 2010-2023. In the above flow chart, we can easily identify how many research articles, conference papers, book chapters, and reviews were published from 2010-2023. This study distinguishes itself from existing literature by offering an all-encompassing and in-depth examination of the Kozeny-Carman model applications specifically concerning permeability dynamics in engineering. While previous studies might have focused solely on theoretical aspects or limited applications within specific engineering domains, this review stands out by providing a comprehensive overview of the model's practical implications across a wide array of engineering disciplines, emphasizing its adaptability and limitations in predicting fluid flow through porous media. Additionally, this study critically evaluates the model's effectiveness in diverse scenarios, offering insights that contribute to a more nuanced understanding of its

utility and fostering innovation in the utilization and refinement of the Kozeny-Carman model within the scientific community.

2. Models of Changes in Permeability Based on Porosity:

Numerous theories have been put forth to examine the relationship between permeability and porosity, as both parameters change simultaneously in laboratory experiments [15,16,17] and [18]. Experimental observations [19] indicate that the permeability of porous media is substantially dependent on the initial state of porosity, the degree of stress, the deformation process (e.g., strain hardening-compaction and strain softening-dilatancy), porous channel geometry, and structure. The power function model and the model of exponential function are the two primary methods among the models that are currently available for the permeability-porosity relationship. The generalized power-law is developed in the log-log and permeability-porosity spaces., is the most widely recognized approach among them. Fig. 4. shows a simple flowchart of models of permeability based on modifications.

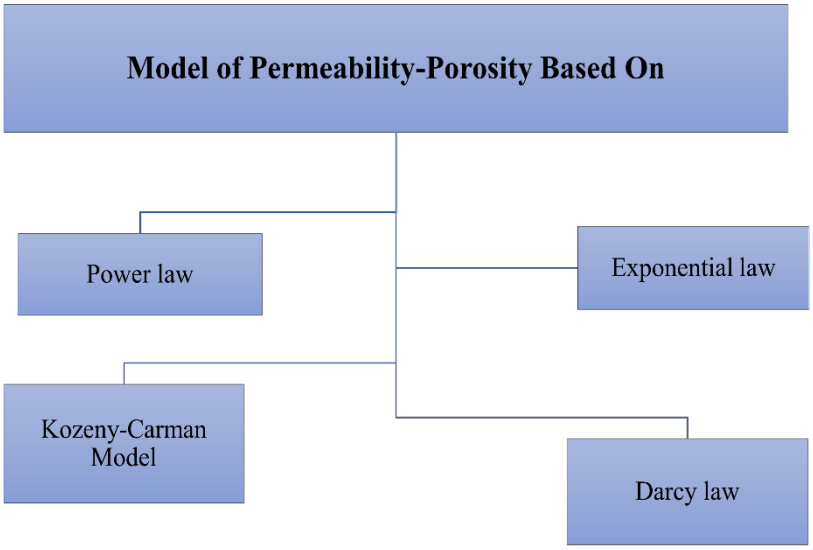

Figure 4. Models of Permeability based on modifications.

2.1. Kozeny–Carman (KC) Model:

The Carman–Kozeny equation (or the Kozeny–Carman equation) is a relation to calculate the pressure A relationship to determine the pressure drop for laminar flow through a packed bed of solids is known as the Carman–Kozeny equation, also known as the Kozeny–Carman equation. According to [20], Kozeny first developed it in 1927 using a simplified model of several parallel capillary tubes with equal lengths and diameters to describe the packed bed. The Kozeny formula can be found by,

$$\frac{\Delta p}{L} = \frac{KV_o\mu}{\phi_s^2 D_p^2}\frac{(1-\varepsilon)^2}{\varepsilon^3}, \quad (1)$$

Where V_o is the superficial or "empty-tower" velocity,Δp is the pressure drop, L is the total height of the bed, μ is the fluid's viscosity, ε is the bed's porosity, ϕ_s is the sphericity of the particles in the packed bed, D_p is the diameter of the equivalent spherical particle, and K is an empirical constant that is dependent on the tortuosity of the bed. A particle's sphericity is determined by,

$$\phi_s = \frac{\left(\frac{6}{D_p}\right)}{a_v}, \quad (2)$$

Where a_v is the particle-specific surface area., the specific surface of the bed is represented by the a_v of the particle if the bed is composed of uniform particles. The particle's a_v can be expressed as the surface-volume ratio, or $a_v = \frac{s_p}{v_p}$, where s_p denotes the particle's surface area and v_p its volume. Thus, $a_v = \frac{6}{D_p}$ and $\phi_s = 1.0$ for a sphere of diameter D_p follow.

Carman determined that $K = 180$ in 1937 by applying Eq. 1 to experimental flow through packed beds results [21]. The value of $K = 150$ was also proposed by other references [22]. According to the Carman–Kozeny equation, the flow is inversely proportional to the fluid viscosity and proportional to the pressure drop. Another name for this assertion, which is frequently used to explain how liquids flow through porous media, is Darcy's law.

2.2. Modifications in the Kozeny-Carman Model in the past:

The Kozeny-Carman (KC) model, which connects porosity and permeability in a general loading space, is one of the most widely used and straightforward models [23] and [24]. One way to put it is as [25].

$$K_p = \frac{\phi^3}{B\tau^2 S^2}, \tag{3}$$

Where K_p is the porous media's permeability, ϕ is its porosity, and τ is its tortuosity, which is the proportion between the actual flow points of flow-in and flow-out actual flow path and their straight path S stands for surface area per unit volume of porous media. The pore shape coefficient, denoted by B, is 2 in the case of circular tubes and 3 in the case of thin cracks. Under some circumstances, this model produces practical simulation results; however, due to the difficult calibration of the pore shape coefficient B and the specific surface area parameter S, it is not a convenient model to use. In order to enhance the evaluation of rock permeability under varied loading circumstances, a number of semi-empirical equations have since been proposed [26] and [27].

On the basis of the fractal pore cross-sectional area, [28] proposed a porosity-permeability relationship that can be expressed as

$$K_p = c\frac{\phi^{z+2}}{(1-\phi)^2}, \tag{4}$$

Another empirical KC-like permeability-porosity model for glass and fiber mats was created in [29], which is expressed as

$$K_p = c\frac{\phi^{z+1}}{(1-\phi)^z}, \tag{5}$$

where z is an exponent variable for porosity and c is a constant for permeability. A comparable permeability formula created by [30] using fractal pore space studies is expressed as

$$K_p = c\frac{\phi^z}{1-\phi}, \tag{6}$$

There are additional empirical and basic functions in this family. For instance, [31] analyzed the low-permeability settling material using a single transient test and a power law:

$$\frac{K_p}{K_o} = \left(\frac{\phi}{\phi_o}\right)^{\alpha}, \quad (7)$$

where α is the porosity-sensitive exponent that is dependent on the properties of the material and its evolution, and K_o and are the initial permeability and porosity, respectively. According to [32], the porosity sensitive exponent for common geological materials ranges from 1 to 25 based on experimental observations. For example, in the analysis by [31], the exponent α equals 11. When [33] measured the permeability in-situ during the hot pressing of calcite, they found that the permeability changes with porosity in the relatively high porosity regime according to a power-law with an exponent of 3. This is consistent with the findings of [34] and Lockner and Evans. Another well-known technique is based on the concept of percolation, which postulates that pore connectivity will vanish if porosity drops below a particular value determined by the percolation threshold. In order to address the permeability-porosity relationship, some researchers have suggested taking percolation theory into account [35], [36], [37], and [38]. [39] used this concept to create a power law of permeability-porosity:

$$K_p = c(\phi - \phi_{cr})^z\,, \quad (8)$$

This simple model has been the subject of numerous research projects. For instance, [15] fit the experimental data of different materials using = 0.04 and z = 2.18; [40] and [41] suggested z = 4.4 and values of 0.0026–0.036 using the "Swiss-Cheese" model. The fully penetrable sphere (FPS) model also proposed z = 2 and = 0.3 by [39], [40], and [43], according to [42]. This model's main flaw is that it requires a series of experimental tests to calibrate its parameters, which are found by measuring the fractal properties of the solid matrix system.

3. Applications of Kozney-Carman model:

3.1.1. Kozeny Carman Equation in Membrane Processing (2011):

In ultrafiltration (UF) and microfiltration (MF) processes, the fluid is transported by means of a pressure differential across the membrane (Δp). The membranes of the UF and MF are permeable with the pore sizes between 0.1 to 10 mm and 2 to 100 nm, in that order [44]. Due

to extremely tiny pore sizes, the idealized flow rate in an cylindrical UF or MF membrane pore that is straight. is regulated by [43]:

$$V = \frac{D^2}{32\mu L_M}, \tag{9}$$

Where L_M is the thickness of the membrane and D is the pore diameter. By multiplying the flow velocity with the fluid density and membrane porosity to find the mass velocity of the fluid (N in $kg \times s^{-1} \times m^{-2}$) through the membrane:

$$N = \frac{\varepsilon \rho D^2}{32\mu L_M} \Delta p, \tag{10}$$

Since the pores in actual porous membranes might not be cylindrical and straight, Eq. 10 can be changed by applying the method created by Carman and Kozeny, in which the hydraulic diameter (D_H) is used in place of the pore diameter:

$$D_H = \frac{4A_p}{P}, \tag{11}$$

Where P is the pore's wetted perimeter and A_p is its cross-sectional area. An alternative expression for D_H can be obtained by expressing A_p and P in terms of the membrane's specific surface area and porosity [43]:

$$D_H = \frac{4\varepsilon}{a_v(1-\varepsilon)}, \tag{12}$$

The true pore length, denoted by L_M, where τ is a tortuosity factor > 1, is longer than the thickness of the membrane. Substituting the tortuosity factor and Eq. 12 in Eq. 10 gives:

$$N = \frac{(\varepsilon^3 \rho)}{2(1-\varepsilon)^2 a_v^2 \mu \tau L_M} \Delta p, \tag{13}$$

An alternate form of the Carman–Kozeny equation is represented by Eq. 13. Using the knowledge that $D_p = \frac{6}{a_v}$ and the actual fluid velocity in the bed $V = \frac{V_o}{\varepsilon}$, Eq. 10 can be rearranged by substituting L_M for L and multiplying by the fluid density ρ.

$$N = \frac{(\varepsilon^3 \rho)}{\left(\frac{K}{36}\right)(1-\varepsilon)^2 a_v^2 \mu L} \Delta p, \tag{14}$$

When Eq. 13 and Eq. 14 are compared with $K = 150$, the result is $\tau = 2.08$; however, when $K = 180, \tau = 2.5$. Stated differently, the Carman–Kozeny equation's empirical constant's numerical value is based on the packed bed's tortuosity, which typically falls between 2.0 and 2.5. The tortuosity in the case of the porous membranes may exceed that of the packed bed. It is possible to determine the porosity and specific surface area of a porous membrane through experimentation. Eq. 13 enables prediction if the membrane tortuosity along the membrane thickness is known. the fluid mass velocity through the membrane under a specific pressure differential acting on the membrane. Alternatively, Eq. 13 can be used to predict the necessary mass fluid velocity given gradient of pressure through the membrane. Bulk-flow permeability (P_M), a gauge of membrane productivity, can also be used to express the mass velocity of fluid through the membrane [43].

$$N = \frac{P_M}{L_M} \Delta p, \tag{15}$$

When we compare Equations 13 and 15, we can see that the bulk-flow permeability in porous UF and MF membranes is provided by

$$P_M = \frac{(\varepsilon^3 \rho)}{2(1-\varepsilon)^2 a_v^2 \mu \tau}, \tag{16}$$

The bulk-flow permeability of microfiltration membranes made by sintering can be predicted using the rearranged version of the original Carman–Kozeny equation, which is provided by Eq. 14. Compressing a powder made of particles of a specific size and sintering it at a high temperature are the steps in this membrane formation process [44]. As a result, the structure of the final membrane resembles that of a packed bed.

Additionally, cake formation on the membrane surface and fluid transport through the membrane can be analyzed using the Carman-Kozeny equation [44]. The fluid leaking through the membrane in this instance needs to get past two barriers in succession: the barrier

preventing the fluid from passing through the cake (R_C) and the barrier preventing the fluid from passing through the membrane (R_M). As a result, the following is an expression for the fluid's mass velocity:

$$N = \frac{\Delta p}{\mu(R_C + R_M)}, \tag{17}$$

And

$$R_C = \left(\frac{K}{36}\right)\frac{(1-\varepsilon)^2 a_v^2 \mu L_C}{\varepsilon^3 \rho}, \tag{18}$$

$$R_M = \frac{2(1-\varepsilon)^2 a_v^2 \mu \tau L_M}{\varepsilon^3 \rho}, \tag{19}$$

The amount of feed processed through the membrane causes the cake thickness (L_c) to increase, which causes R_c to increase in proportion. If there is no adsorption of solute particles inside the membrane pores, R_M remains constant. Equations 17, 18, and 19 are similar to the ones that explain the traditional cake filtration method.

3.1.2. Kozeny–Carman Model Application in Predicting the Acoustical Properties of Polyester Fiber (2015):

Fibers made of polyester are effective at absorbing sound [45]. Panels with acoustic absorption made of polyester fibers are increasingly widely used in industrial, automotive, and building noise control applications; they rival conventional mineral fiber absorbers in these markets. Since Polyester fiber is a material that has a high porosity, which is typically higher than $\phi \geq 0.97$. Numerous uses for polyester fiber is compressed, changing the bulk material density in the process, and porousness. While the alteration in material characteristics is typically minimal, it has a substantial impact on the fibers' flow resistivity. the factor that primarily accounts for their fundamental sound characteristics.

This study shows that the flow resistivity alone can be used to predict the acoustical properties of polyester fibers using a simpler model. Furthermore, demonstrated is the flow resistivity is connected theoretically to the bulk material density and fiber diameter using the method

recommended by Carman and Kozeny [46,47] in early 1930s. This method seems more tangible and offers a a more precise estimation of polyester fiber's flow resistivity based on the data on fiber diameter and density.

As was previously discussed in 2015 [48], this section shows that the acoustical properties of polyester fibers can be predicted using a simpler model that is based only on flow resistivity. It is also demonstrated that, by applying the method proposed by Carman and Kozeny [46,47] in the 1930s, the flow resistivity is theoretically related to the fiber diameter and bulk material density. This method looks more tangible and uses data on fiber density and diameter to estimate polyester fiber flow resistivity more precisely.

Polyester fibers with a mean diameter ranging from 20.2 μm to 39.2 μm were the subject of this investigation. A magnified image of polyester fibers with a diameter of roughly 25 μm is shown in Fig. 5. In the textile industry, polyester fibers are generally arranged based on their Denier, a unit of measurement for linear mass density that is defined as the mass in grammes per 9000 m.

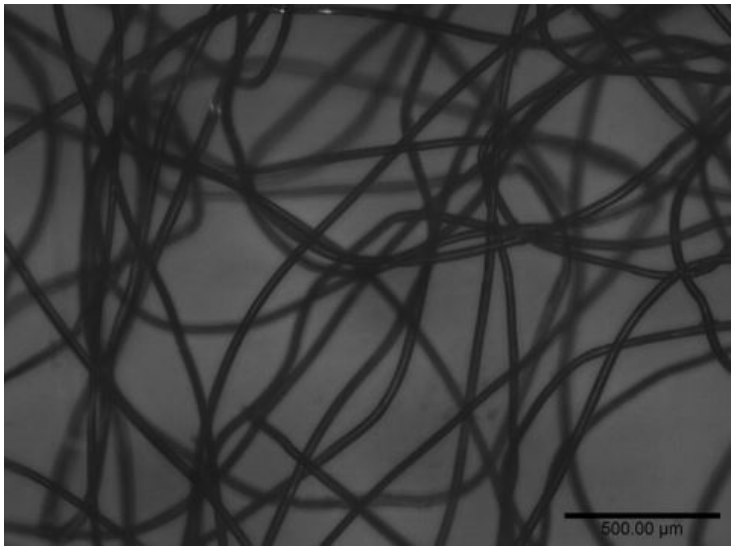

Figure 5. A photograph of polyester fibers with 24.8 µm diameter (adapted from Ref. [50]).

Determining the physical parameters (airflow resistivity, open porosity, tortuosity, and viscous and thermal characteristic lengths) in the modeling of the acoustical behavior of highly porous materials can be a laborious procedure [48]. As such, inverse methodologies are increasingly being used to obtain the desired characteristic parameters [49]. This paper's work is based solely on the inversion of flow resistivity from data on the acoustic absorption coefficient from an experiment

using two microphone impedance tubes. Ref. [50] provides a detailed method for determining the acoustic absorption coefficient. The experiment described in this paper measured the polyester fiber samples absorption coefficients at various bulk densities, from which the flow resistivity values are expanded upon. The bulk densities used in the tests for each sample were 40.1 $kg/m^3$22.8, 24.4, and 32.9. Fig. 6 shows the 100 mm impedance tube that was used for this measurement.

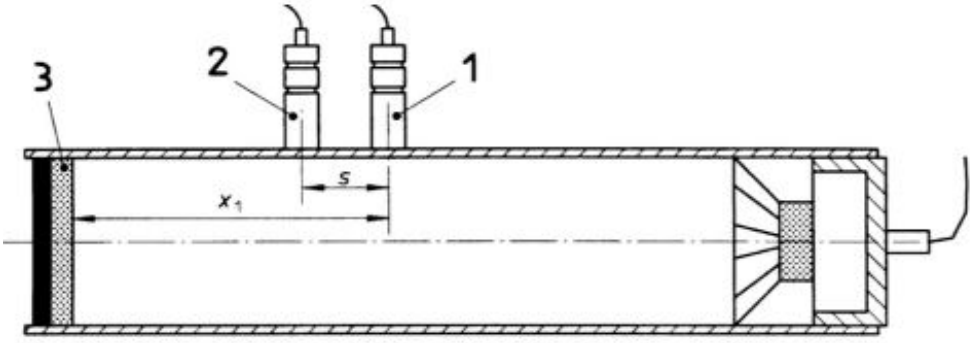

Key
1 Microphone A
2 Microphone B
3 Test specimen

Figure 6. Impedance tube arrangement (adapted from Ref. [50]).

The density of the polyester fiber sample in the tube was adjusted using the sample holder with an adjustable piston by changing the sample length l_s for a specific mass of fibers in the sample and then taking an acoustic measurement. This allowed for the measurement of the acoustic absorption coefficient of a hard-back polyester fiber sample across a range of material densities and frequency ranges, from 100 to 1600 Hz. By utilizing the indirect method of parameter inversion, which is predicated on locating the minimum of the subsequent function, the flow resistivity was extracted from the acoustic absorption coefficient data:

$$F(\sigma) = \sum_n |\alpha_e(f_n) - \alpha_m(f_n, \sigma)|, \quad (20)$$

where σ is airflow resistivity, f_n is the sound frequency, and α_e is the experimental absorption coefficient $\alpha_m$is the predicted absorption coefficient. The 1-parameter Miki model [54], which

predicts the absorption coefficient α_m, was used to predict the complex wavenumber and characteristic impedance with the following expressions:

$$z_b(f) = \left\{1 + 0.070\left(\frac{f}{\sigma}\right)^{-0.632} + 0.0107i\left(\frac{f}{\sigma}\right)^{-0.632}\right\}, \tag{21}$$

and

$$k_b(f) = \frac{2\pi f}{c_0}\left\{1 + 0.109\left(\frac{f}{\sigma}\right)^{-0.618} + 0.160i\left(\frac{f}{\sigma}\right)^{-0.618}\right\}, \tag{22}$$

respectively. Here, c_0 is the speed of sound in air and $i = \sqrt{-1}$. The absorption coefficient for a polyester fibre specimen with a hard backing can be found using the following expression:

$$\alpha = 1 - \left|\frac{Z_s - 1}{Z_s + 1}\right|^2, \tag{23}$$

where Z_s is the hard backed layer polyester fiber sample of thickness l_s normalized acoustic surface impedance, which is provided by:

$$Z_s = Z_b \coth\left(-ik_b l_s\right), \tag{24}$$

The optimization technique Nelder-Mead simplex (direct search) [53] was employed in this work to address the minimization problem given by Eq. (1). This made it possible for us to determine the flow resistivity value that provided the best fit between the values predicted by the Miki model and the absorption coefficient values discovered in the experiment reported [52]. Fig. 7 compares the absorption coefficient observed with the one predicted using the optimized value of flow resistivity. The maximum mean error between the measured parameters and the suggested parameter inversion procedure and predicted absorption coefficient spectra was below 0.5%.

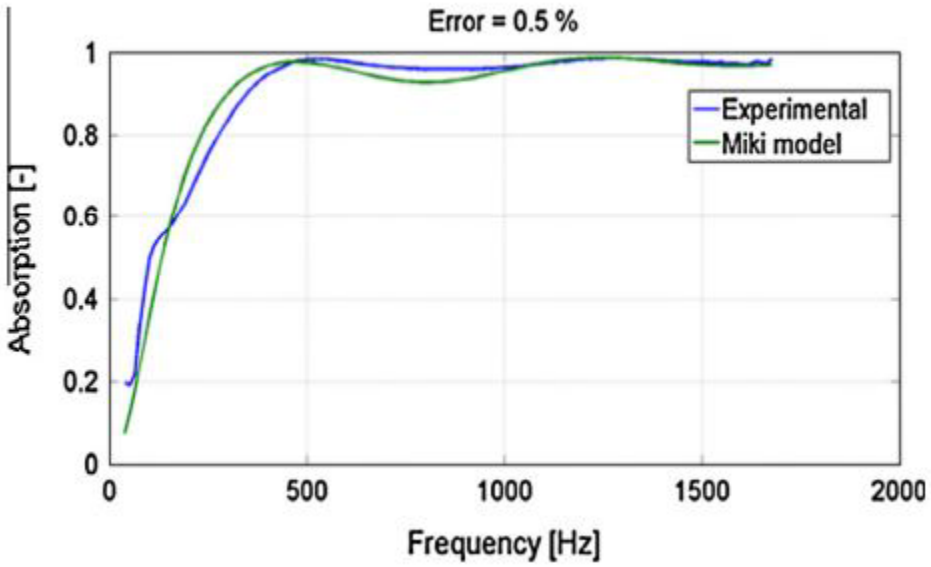

Figure 7. The absorption coefficient for a 200 mm hard-backed layer of polyester fibers with a diameter of 39.2 mm and a bulk density of 24.4 kg/m^3 is both predicted and measured (adapted from Ref. [50]).

The Kozeny-Carman equation, which was employed in this work, was created in the 1930s to establish a relationship between the flow resistivity, σ, particle size, d, and porosity of granular media, ϕ.

$$\sigma = \frac{180\mu(1-\phi)^2}{d^2\phi^3}, \tag{25}$$

The Poiseuille equation for laminar fluid flow with the dynamic viscosity, μ, can be used to derive this physical relation. The particle diameter in Eq. (25) can be set to the fiber diameter $d = d_f$ in the case of a medium made up of fibers with diameter d_f. The ratio of the bulk material density, ρ_m, to the polyester fiber density, ρ_f, can be used to estimate the porosity in Eq. (25).

$$\phi = 1 - \left(\frac{\rho_m}{\rho_f}\right), \tag{26}$$

It is a quantity that can be measured directly. The density of the polyester fiber used in this study's experiments is 1380 kg/m^3, which is consistent with typical polyester density values and was supplied by our supplier. If we clarify:

$$\gamma = \frac{(1-\phi)^2}{\phi^3}, \tag{27}$$

The airflow resistivity is therefore a linear function whose slope depends inversely on d_f^2, according to the Kozeny–Carman equation, i.e.:

$$\sigma = \left(\frac{180\mu}{d_f^2}\right)\gamma, \tag{28}$$

3.1.3. Kozeny–Carman Model Application in Predicting Building Foundation of Clay Soil (2022)

The most basic building material for a foundation is soil. The safety of the buildings is directly correlated with the engineering qualities of the soil. For example, the mechanics and permeability properties of the soil directly affect the configuration of supports in the building foundation pit and the groundwater treatment [54-56]. One example of how the foundation settles later due to secondary consolidation of the soil is the leaning Bisha Tower [57-59]. This directly affects the buildings' ability to be used safely. The above issues solutions are all closely related to the soil's hydraulic conductivity, a crucial component of soil permeability. Since hydraulic conductivity is directly correlated with soil structures, porosity, bulk density, saturation, and fluid type, it is regrettably a challenging parameter to measure [60,61]. As a result, numerous permeability calculation techniques and prediction models have been put forth by academics [47, 60-75]. Nonetheless, the K-C equation and Darcy's law continue to be the most frequently utilized.

The primary constituents of clay are clay minerals, including illite, kaolinite, and montmorillonite. The majority of these mineral crystals consist of sheets of gibbsite, brucite, and silicon.. However, isomorphous substitution in all clay minerals results in a net negative charge for the clay particles because the bonds holding the unit layers together may be sufficiently weak and easily influenced by the environment [76]. DEL is created when polar water molecules and cations are adsorbent by the net negative charges (Figure 8). Strongly adsorbed water is defined by some academics as multiple layers of water molecules adsorbed on the particle surface; they contend that strongly adsorbed water is incapable of flowing [77]. Many clay particles are tiny flakes that are influenced by the crystal structure of clay minerals. The flakes are stacked in different ways during deposition because of the interaction of van der Waals, gravity, and electric field forces. The clay's pore structure is altered by this haphazard stack (Figure 9). Among them are isolated pores and blind

pores, which are self-locking and prevent water from passing through them. However, because of the DEL and the adsorbed water, some tiny pores, like the gaps between the flakes, still prevent liquid from passing through them even though they are connected [78]. As a result, clay seepage is not permitted through any of these tiny pores, the above isolated pores, or the blind pores.

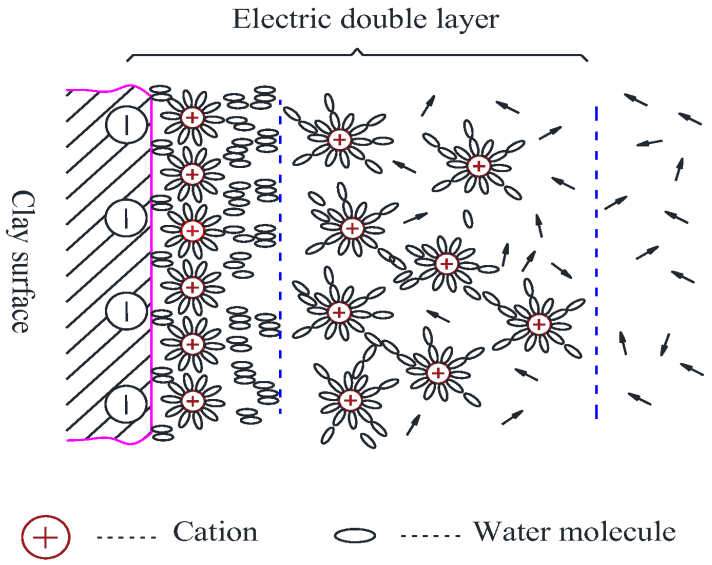

Figure 8. Schematic diagram of diffuse electric double layer (adapted from Ref. [80]).

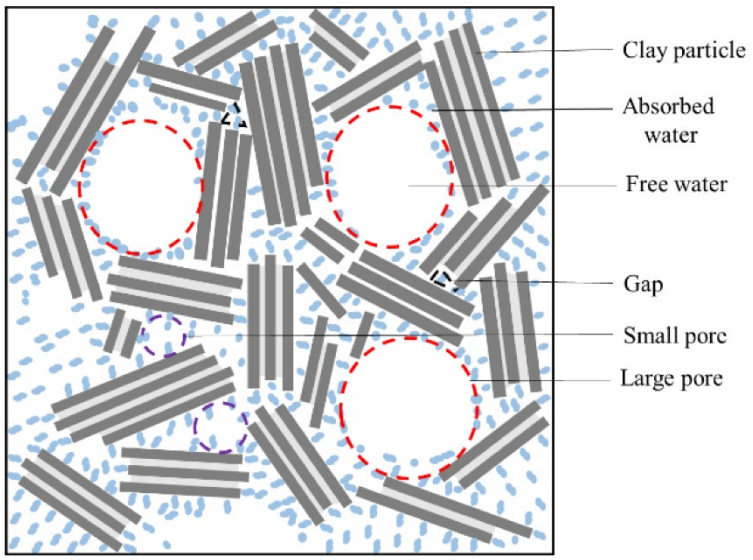

Figure 9. Pore structure of clay in microscope (adapted from Ref. [80]).

Using Poiseuille's law as a modification, a permeability prediction model for a capillary displays the average flow velocity v_{ave} as follows:

$$v_{ave} = \frac{\gamma_p R^2}{8\mu} i_h, \tag{29}$$

where i_h is the hydraulic gradient, γ_p is the specific gravity, R is the tube's radius, and μ is the viscosity (Figure 10). The hydraulic radius of a circular tube with full flow is:

$$R_H = \frac{\pi R^2}{2\pi R} = \frac{R}{2}, \tag{30}$$

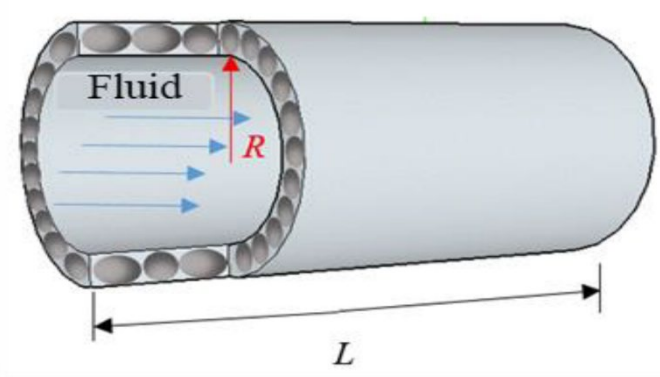

Figure 10. Tube model of soil seepage (adapted from Ref. 80]).

Poiseuille's formula can now be used to determine the fluid volume of the tube, which is as follows:

$$q_{cir} = \frac{\gamma_p R_H^2 i_h a}{2\mu}, \tag{31}$$

where a is the tube's cross-sectional area. When the shape factor C_s is added, the previous formula takes on the following form for pores with varying shapes:

$$q_{cir} = C_s \frac{\gamma_p R_H^2 i_h a}{\mu}, \tag{32}$$

The area of flow passages in saturated soils with a total cross-sectional area of A is equal to A_f.

$$A_f = nA, \tag{33}$$

where n is the soil's porosity. The hydraulic radius, or R_H, can also be written as:

$$R_H = \frac{A_f}{P_c} = \frac{A_f L_f}{P_c L_f} = \frac{V_w}{V_s \rho_s S_p}, \quad (34)$$

where V_w and V_s are the volume of water and solid, respectively, and ρ_s is the density of soil particles. P_c is the total circumference of the flow tubes. L_f is the length of the flow tube. Since clay has interconnected pores and fluid can only flow through them, S_p in this formula represents the SSA of the pores—that is, the SSA of particles along the interconnected pores that allow liquid to flow through them efficiently. Equation (33) can now be expressed as follows:

$$q = C_s \frac{\gamma_p}{\mu} \left(\frac{V_w}{V_s \rho_s S_p} \right) i_h A_f, \quad (35)$$

Apart from unconnected pores, absorbed water, and small pores affected by absorbed water but not contributing to seepage are all considered invalid in this paper and are not included in the effective e calculation [60,77]. The following formula is used to determine the volume of adsorbed water:

$$V_{ab} = \delta . S_p, \quad (36)$$

where S_p is the SSA and δ is the adsorbed water thickness. Given that a single water molecule has a diameter of $0.3\ nm$ [77], the effective radius of the tube becomes $R - 0.6\ nm$ or $R - 0.9\ nm$ if there are two or three layers of adsorbed water molecules on the particle surface. Simultaneously, the Gouy-Chapman theory states that the natural soil ion concentration ranges from $0.83 \times 10^{-2}\ mol/L$ to $0.83 \times 10^{-4}\ mol/L$ [76]. Figure 7 shows the thicknesses of DEL as $3.33\ nm$ and $33.3\ nm$, however not all of the liquids in the DEL are unable to flow.

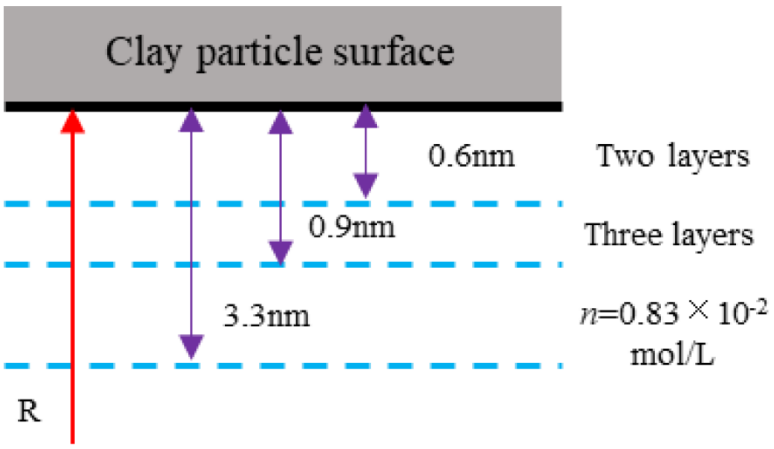

Figure 11. Influence of absorbed water or DEL (adapted from Ref. [56]).

Considering the considerations, pores with a diameter of less than 3 nm are regarded as invalid pores in this work since they are affected by absorbed water but do not contribute to seepage. Currently, the amount of clay pores that positively contribute to seepage can be expressed as follows:

$$V_v' = V_v - V_{ab} - V_{unc} - V_{noc} \tag{37}$$

Where V_{unc} is the volume of unconnected pores, such as blind and isolated pores, which can be measured using the MIP test; V_v' is the effective pore volume; and V_{noc} is the volume of pores affected by absorbed water and with no contribution to seepage. Next, the interconnected pores' effective e_{eff} is displayed as follows:

$$e_{eff} = \frac{V_v'}{V_s'} = \frac{V_v - V_{ab} - V_{unc} - V_{noc}}{V_s + V_{ab}} \tag{38}$$

Where V_s' is the volume of soil particles plus the volume of water that has been adsorbed, and V_s is the volume of soil particles. Currently, there is:

$$V_w = e_{eff} V_s' = e_{eff}(V_s + V_{ab}), \tag{39}$$

The SSA of the particles along the connected pores can be expressed as effective SSA (Seff) after removing the pores with diameters smaller than $3\ nm$. The hydraulic conductivity under stable laminar flow can be found using Darcy's law by changing the V_s to V_s' and substituting Equations (33), (38), and (39) into Equation (36):

$$k = C_s \frac{\gamma_p}{\mu} \left(\frac{e_{eff}(V_s+V_{ab})}{(V_s+V_{ab})\rho_s S_{eff}} \right)^2 \frac{e_{eff}}{1+e_{eff}} = C_s \frac{\gamma_p}{\mu \rho_s^2 S_{eff}^2} \frac{e_{eff}^3}{(1+e_{eff})}, \quad (40)$$

It is challenging to determine the precise value of the coefficient C_s, which describes the tortuosity of pores in the formula. Currently, experience plays a major role in selecting this coefficient. The works of Mitchell and Soga [76] state that C_s is assumed to be 5 in this model. The formula becomes the traditional K-C equation when S_{eff} and e_{eff} are interpreted as the specific surface area S and total pore e, respectively.

4. Concluiding Remarks:

For a conclusion, this review article analysis shows the significance the Kozeny-Carman (KC) model is for figuring out the complicated mechanics of permeability in engineering domains. This review points out the model wide applications in a range of engineering domains. We can conclude our discussuion with these following important points:

1. For a conclusion, this review article analysis shows the significance the Kozeny-Carman (KC) model is for figuring out the complicated mechanics of permeability in engineering domains. This review points out the model wide applications in a range of engineering domains. We can conclude our discussuion with these following important points:
2. This review shows the KC model wide application by showing its significance and applicability in multiple engineering domains. In numerous diverse applications from engineering to geotechnical processes, such as petroleum engineering to civil engineering, this model has flexibility and effectiveness .
3. This comprehensive review shows that the model is used by researchers and engineers as a guidance when addressing complicated permeability-related issues in many different kinds of engineering applications.

4. The Kozeny-Carman model, despite being a widely accepted theoretical framework for predicting fluid flow through porous media, faces challenges in direct real-world applications due to several reasons. One primary factor is the model's simplifications and assumptions, which might not fully capture the complexity and heterogeneity of real porous materials. The model assumes uniformity in pore size, shape, and packing, which often doesn't hold true in practical applications where porous media exhibit significant variability. Moreover, obtaining accurate input parameters for the model, such as porosity and tortuosity, can be challenging and often requires complex experimental measurements that might not always be feasible or readily available. Consequently, while the model serves as a valuable predictive tool in theoretical studies and simulations, its direct application in real-world scenarios is limited by these simplifications and the difficulty in acquiring precise parameters, leading to more prevalent use in predictive modeling rather than direct practical applications. Researchers continuously work on refining and adapting the model to enhance its applicability in diverse real-world settings.

5. Future Prospectives:

For future prospectives we have a some points which is help for engineers and researchers in finding the right solution for engineering issues.

1. To Investigate the improvement of the Kozeny-Carman (KC) model parameters for more accuracy for complex porous media.
2. To Investigate combining cutting-edge technologies such as computational fluid dynamics (CFD) or machine learning with the KC model.
3. To improve the KC model stability in various engineering applications, for some experimental validation.
4. To gain a deeper understanding of how environmental factors affect permeability dynamics, explore including them as well.
5. Encourage interdisciplinary cooperation to expand the KC model applicability and enhance its capabilities.

Declarations: It is declared that there is no conflict of interest for this research.

Data Availability: All the data related to this research is included in the manuscript.

Funding: There is no source of funding for this research.

References:

1. Friedman, M. (1976, August). Porosity, permeability, and rock mechanics-a review. In ARMA US Rock Mechanics/Geomechanics Symposium (pp. ARMA-76). ARMA.
2. Berkowitz, B. (2002). Characterizing flow and transport in fractured geological media: A review. Advances in water resources, 25(8-12), 861-884.
3. Zhu, W., & Wong, T. F. (1997). The transition from brittle faulting to cataclastic flow: Permeability evolution. Journal of Geophysical Research: Solid Earth, 102(B2), 3027-3041.
4. Morris, J. P., Lomov, I. N., & Glenn, L. A. (2003). A constitutive model for stress-induced permeability and porosity evolution of Berea sandstone. Journal of Geophysical Research: Solid Earth, 108(B10).
5. Shoaib, Muhammad, et al. "Variational iteration method along with intelligent computing system for the radiated flow of electrically conductive viscous fluid through porous medium." *Heliyon* 9.3 (2023).
6. Jawad, M., Hameed, M. K., Nisar, K. S., & Majeed, A. H. (2023). Darcy-Forchheimer flow of maxwell nanofluid flow over a porous stretching sheet with Arrhenius activation energy and nield boundary conditions. *Case Studies in Thermal Engineering*, *44*, 102830.
7. Singh, B., & Nisar, K. S. (2023). Thermal instability of magnetohydrodynamic couple stress nanofluid in rotating porous medium. *Numerical Methods for Partial Differential Equations*, *39*(6), 4454-4467.
8. Reddy, Y. D., Goud, B. S., Nisar, K. S., Alshahrani, B., Mahmoud, M., & Park, C. (2023). Heat absorption/generation effect on MHD heat transfer fluid flow along a stretching cylinder with a porous medium. *Alexandria Engineering Journal*, *64*, 659-666.
9. Nisar, K. S., Anjum, M. W., Raja, M. A. Z., & Shoaib, M. (2023). Homogeneous-heterogeneous reactions on Darcy-Forchheimer nanofluid flow system. *Case Studies in Thermal Engineering*, 103882.

10. Nisar, K. S., Shoaib, M., Raja, M. A. Z., Tariq, Y., Rafiq, A., & Morsy, A. (2023). Design of neural networks for second-order velocity slip of nanofluid flow in the presence of activation energy. *AIMS Mathematics*, *8*(3), 6255-6277.
11. Zubair, T., Usman, M., Nisar, K. S., Hamid, M., Mahmoud, E. E., & Yahia, I. S. (2022). Investigation of shape effects of Cu-nanoparticle on heat transfer of MHD rotating flow over nonlinear stretching sheet. Alexandria Engineering Journal, 61(6), 4457-4466.
12. Rashid, I., Zubair, T., Asjad, M. I., Irshad, S., & Eldin, S. M. (2023). The MHD graphene− CMC− water nanofluid past a stretchable wall with Joule heating and velocity slip impact: Coolant application. Frontiers in Physics, 10, 1278.
13. Liaqat, M.I., Akgül, A. & Bayram, M. (2024). Series and closed form solution of Caputo time-fractional wave and heat problems with the variable coefficients by a novel approach. *Opt Quant Electron* **56**, 203.
14. Partohaghighi, Mohammad & Mortezaee, Marzieh & Akgül, Ali & Hassan, Ahmed & Sakar, Necibullah. (2024). Numerical analysis of the fractal-fractional diffusion model of ignition in the combustion process. Alexandria Engineering Journal. 86.
15. Zhang, S., Cox, S. F., & Paterson, M. S. (1994). The influence of room temperature deformation on porosity and permeability in calcite aggregates. Journal of Geophysical Research: Solid Earth, 99(B8), 15761-15775.
16. Schutjens, P. M., Hanssen, T. H., Hettema, M. H. H., Merour, J., de Bree, J. P., Coremans, J. W. A., & Helliesen, G. (2001, September). Compaction-induced porosity/permeability reduction in sandstone reservoirs: Data and model for elasticity-dominated deformation. In SPE Annual Technical Conference and Exhibition? (pp. SPE-71337). SPE.
17. Zhu, W., Montési, L. G., & Wong, T. F. (2007). A probabilistic damage model of stress-induced permeability anisotropy during cataclastic flow. Journal of Geophysical Research: Solid Earth, 112(B10).
18. Hu, D. W., Zhou, H., Zhang, F., & Shao, J. F. (2010). Evolution of poroelastic properties and permeability in damaged sandstone. International Journal of Rock Mechanics and Mining Sciences, 47(6), 962-973.
19. Sulem, J., & Ouffroukh, H. (2006). Shear banding in drained and undrained triaxial tests on a saturated sandstone: Porosity and permeability evolution. International Journal of Rock Mechanics and Mining Sciences, 43(2), 292-310.

20. McCabe, W. L., Smith, J. C., & Harriott, P. (1993). Unit operations of chemical engineering. McGraw-hill.
21. Foust, A. S., Wenzel, L. A., Clump, C. W., Maus, L., & Andersen, L. B. (2008). Principles of unit operations. John Wiley & Sons.
22. Seader, J. D., Henley, E. J., & Roper, D. K. (2006). Separation process principles.
23. Kozeny, J. (1927). Ueber kapillare leitung des wassers im boden. Sitzungsberichte der Akademie der Wissenschaften in Wien, 136, 271.
24. Carman, P. C. (1937). Fluid flow through a granular bed. Trans. Inst. Chem. Eng. London, 15, 150-156.
25. Walsh, J. B., & Brace, W. F. (1984). The effect of pressure on porosity and the transport properties of rock. Journal of Geophysical Research: Solid Earth, 89(B11), 9425-9431.
26. Panda, M. N., & Lake, L. W. (1994). Estimation of single-phase permeability from parameters of particle-size distribution. AAPG bulletin, 78(7), 1028-1039.
27. Bernabé, Y., Mok, U., & Evans, B. (2003). Permeability-porosity relationships in rocks subjected to various evolution processes. Pure and Applied Geophysics, 160, 937-960.
28. Bayles, G. A., Klinzing, G. E., & Chiang, S. H. (1989). Fractal mathematics applied to flow in porous systems. Particle & Particle Systems Characterization, 6(1-4), 168-175.
29. Rodriguez, E., Giacomelli, F., & Vazquez, A. (2004). Permeability-porosity relationship in RTM for different fiberglass and natural reinforcements. Journal of composite materials, 38(3), 259-268.
30. Costa, A. (2006). Permeability-porosity relationship: A reexamination of the Kozeny-Carman equation based on a fractal pore-space geometry assumption. Geophysical research letters, 33(2).
31. Ghabezloo, S., Sulem, J., & Saint-Marc, J. (2009). Evaluation of a permeability–porosity relationship in a low-permeability creeping material using a single transient test. International Journal of Rock Mechanics and Mining Sciences, 46(4), 761-768.
32. David, C., Wong, T. F., Zhu, W., & Zhang, J. (1994). Laboratory measurement of compaction-induced permeability change in porous rocks: Implications for the generation and maintenance of pore pressure excess in the crust. pure and applied geophysics, 143, 425-456.

33. Zhang, S., Paterson, M. S., & Cox, S. F. (1994). Porosity and permeability evolution during hot isostatic pressing of calcite aggregates. Journal of Geophysical Research: Solid Earth, 99(B8), 15741-15760.
34. Zhu, W., David, C., & Wong, T. F. (1995). Network modeling of permeability evolution during cementation and hot isostatic pressing. Journal of Geophysical Research: Solid Earth, 100(B8), 15451-15464.
35. Dienes, J. K. (1982, August). Permeability, percolation and statistical crack mechanics. In ARMA US Rock Mechanics/Geomechanics Symposium (pp. ARMA-82). ARMA.
36. Zhang, S., Cox, S. F., & Paterson, M. S. (1994). The influence of room temperature deformation on porosity and permeability in calcite aggregates. Journal of Geophysical Research: Solid Earth, 99(B8), 15761-15775.
37. Guéguen, Y., Chelidze, T., & Le Ravalec, M. (1997). Microstructures, percolation thresholds, and rock physical properties. Tectonophysics, 279(1-4), 23-35.
38. Alkan, H. (2009). Percolation model for dilatancy-induced permeability of the excavation damaged zone in rock salt. International Journal of Rock Mechanics and Mining Sciences, 46(4), 716-724.
39. Sahimi, M. (1994). Applications of percolation theory. CRC Press.
40. Sornette, D. (1987). Difference between lattice and continuum failure threshold in percolation. Journal de Physique, 48(11), 1843-1847.
41. Saar, M. O., & Manga, M. (1999). Permeability-porosity relationship in vesicular basalts. Geophysical Research Letters, 26(1), 111-114.
42. Seader JD, Henley EJ, Roper DK (2011) Separation process principles. Wiley, Hoboken
43. Mulder M (1996) Basic principles of membrane technology. Kluwer, Dordrecht
44. Narang P. Material parameter selection in polyester fibre insulation for sound transmission and absorption. Appl Acoust 1995;45(4):335–58.
45. Kino N, Ueno T. Evaluation of acoustical and non-acoustical properties of sound absorbing materials made of polyester fibres of various cross-sectional shapes. Appl Acoust 2008;69(7):575–82.
46. Kozeny J. Über kapillare Leitung des Wassers im Boden: (Aufstieg, Versickerung und Anwendung auf die Bewässerung), Hölder-PichlerTempsky; 1927.
47. Carman P. Fluid flow through granular beds. Chem Eng Res Des 1997;75:S32–48.

48. Bonfiglio P, Pompoli F. Inversion problems for determining physical parameters of porous materials: overview and comparison between different methods. Acta Acust Acust 2013;99(3):341–51.
49. Pelegrinis, M. T., Horoshenkov, K. V., & Burnett, A. (2016). An application of Kozeny–Carman flow resistivity model to predict the acoustical properties of polyester fibre. *Applied Acoustics*, *101*, 1-4.
50. ISO, 10534-2: Acoustics. Determination of sound absorption coefficient and impedance in impedance tubes. Transfer-function method, 2009.
51. Miki Y. Acoustical properties of porous materials. modifications of delanybazley models. J Acoust Soc Jpn (E) 1990;11(1):19–24.
52. Nelder JA, Mead R. A simplex method for function minimization. Comput J 1965;7(4):308–13.
53. Chen, J., Tong, H., Yuan, J., Fang, Y., & Gu, R. (2022). Permeability Prediction Model Modified on Kozeny-Carman for Building Foundation of Clay Soil. *Buildings*, *12*(11), 1798.
54. Chang, W.; Wang, P.; Wang, H.; Chai, S.; Yu, Y.; Xu, S. Simulation of the Q(2) loess slope with seepage fissure failure and seismic response via discrete element method. Bull. Eng. Geol. Environ. **2021**, 80, 3495–3511.
55. Dong, H.; Huang, R.; Gao, Q. Rainfall infiltration performance and its relation to mesoscopic structural properties of a gravelly soil slope. Eng. Geol. **2017**, 230, 1–10.
56. Jie, Y.X.; Jie, G.; Mao, Z.; Li, G. Seepage analysis based on boundary-fitted coordinate transformation method. Comput. Geotech. **2004**, 31, 279–283.
57. Yao, Z.; Chen, Z.; Fang, X.; Wang, W.; Li, W.; Su, L. Elastoplastic damage seepage-consolidation coupled model of unsaturated undisturbed loess and its application. Acta Geotech. **2020**, 15, 1637–1653.
58. Ba-Phu, N.; Kim, Y. An analytical solution for consolidation of PVD-installed deposit considering nonlinear distribution of hydraulic conductivity and compressibility. Eng. Comput. **2019**, 36, 707–730.
59. Pane, V.; Croce, P.; Znidarcic, D.; Ko, H.-Y.; Olsen, H.W.; Schiffman, R.L. Effects of consolidation on permeability measurements for soft clay. Géotechnique **1983**, 33, 67–72.

60. Ren, X.; Zhao, Y.; Deng, Q.; Kang, J.; Li, D.; Wang, D. A relation of hydraulic conductivity—Void ratio for soils based on Kozeny-carman equation. Eng. Geol. **2016**, 213, 89–97.
61. Chapuis, R.P. Predicting the saturated hydraulic conductivity of soils: A review. Bull. Eng. Geol. Environ. **2012**, 71, 401–434.
62. Zhang, F.; Wang, T.; Liu, F.; Peng, M.; Bate, B.; Wang, P. Hydro-mechanical coupled analysis of near-wellbore fines migration from unconsolidated reservoirs. Acta Geotech. **2022**, 17, 3535–3551.
63. Wang, M.; Wang, J.; Xu, G.; Zheng, Y.; Kang, X. Improved model for predicting the hydraulic conductivity of soils based on the Kozeny–Carman equation. Hydrol. Res. **2021**, 52, 719–733.
64. Hong, B.; Li, X.; Wang, L.; Li, L.; Xue, Q.; Meng, J. Using the effective void ratio and specific surface area in the Kozeny-Carman Equation to predict the hydraulic conductivity of loess. Water **2020**, 12, 24.
65. Jang, J.; Narsilio, G.A.; Santamarina, J.C. Hydraulic conductivity in spatially varying media—A pore-scale investigation. Geophys. J. Int. **2015**, 184, 1167–1179.
66. Chai, J.C.; Agung, P.M.A.; Hino, T.; Igaya, Y.; Carter, J.P. Estimating hydraulic conductivity from piezocone soundings. Geotechnique **2011**, 8, 699–708.
67. Costa, A. Permeability-porosity relationship: A reexamination of Kozeny-Carman equation based on a fractal pore-space geometry assumption. Geophys. Res. Lett. **2006**, 33, 87–94.
68. Asger, M.N.; Fridolin, O.; Henrik, B. Reexamination of Hagen-Poiseuille flow: Shape dependence of the hydraulic resistance in microchannels. Phys. Rev. E **2005**, 71, 057301.
69. Chapuis, R.P.; Legare, P.P. A simple method for determining the surface area of fine aggregates and fillers in bituminous mixtures. In Proceedings of the Effects of Aggregates and Mineral Fillers on Asphalt Mixture Performance, San Diego, CA, USA, 10 December 1991; pp. 177–186.
70. Samarasinghe, A.M.; Huang, Y.H.; Drnevich, V.P. Permeability and consolidation of normally consolidated soils. J. Geotech. Eng. Div. **1982**, 108, 835–850.
71. Childs, E.C. Dynamics of fluids in Porous Media. Eng. Geol. **1972**, 7, 174–175.

72. Mesri, G.; Olson, R.E. Consolidation characteristics of montmorillonite. Geotechnique **1971**, 4, 341–352.
73. Taylor, D.W. Fundamentals of soil mechanics. Soil Sci. **1948**, 66, 161.
74. Carman, P.C. Permeability of saturated sands, soils and clays. J. Agric. Sci. **1939**, 2, 12.
75. Carman, P.C. Fluid flow through granular beds. Chem. Eng. Res. Des. **1937**, 75, S32–S48.
76. Kozeny, J. Uber Kapillare Leitung des Wassers im Boden. Sitzungsber. Akad. Wiss. **1927**, 136, 271–306.
77. Mitchell, J.K.; Soga, K. Fundamentals of Soil Behavior, 3rd ed.; John Wiley & Sons: Hoboken, NJ, USA, 2005.
78. Singh, P.N.; Wallender, W.W. Effects of adsorbed water layer in predicting saturated hydraulic conductivity for clays with Kozeny–Carman equation. J. Geotech. Geoenvironmental Eng. **2008**, 134, 829–836.
79. Chen, J.; Fang, Y.; Gu, R.; Shu, H.; Ba, L.; Li, W. Study on pore size effect of low permeability clay seepage. Arab. J. Geosci. **2019**, 12, 238.